In-Situ Catalytic Surface Modification of Micro-Structured La$_{0.6}$Sr$_{0.4}$Co$_{0.2}$Fe$_{0.8}$O$_{3-\delta}$ (LSCF) Oxygen Permeable Membrane Using Vacuum-Assisted technique

Nur Hidayati Othman[1], Munawar Zaman Shahruddin[1], 'Ainun Sailah Sihar[1], Zhentao Wu[2] and K. Li[2]

[1]*Department of Oil and Gas Engineering, Faculty of Chemical Engineering, Universiti Teknologi MARA, 4050 Shah Alam, Malaysia*
[2]*Department of Chemical Engineering, Imperial College London, London SW7 2AZ, UK*

Abstract. This paper aims at investigating the means to carry out in-situ surface modification of La$_{0.6}$Sr$_{0.4}$Co$_{0.2}$Fe$_{0.8}$O$_{3-\delta}$ (LSCF) oxygen permeable membrane by using vacuum assisted technique. The unique structure of the LSCF hollow fibre membrane used in this study, which consists of an outer dense oxygen separation layer and conical-shaped microchannels open at the inner surface has allowed the membrane to be used as oxygen separation membrane and as a structured substrate for where catalyst can be deposited. A catalyst solution of similar material, LSCF was prepared using sol-gel technique. Effects of calcination temperature and heating rate were investigated using XRD and TGA to ensure pure perovskites structure of LSCF was obtained. It was found that a lower calcination temperature can be used to obtain pure perovskite phase if slower heating rate is used. The SEM photograph shows that the distribution of catalyst onto the membrane microchannels using in-situ deposition technique was strongly related to the viscosity of LSCF catalytic sol. Interestingly, it was found that the amount of catalyst deposited using viscous solution was slightly higher than the less viscous sol. This might be due to the difficulty of catalyst sol to infiltrate the membrane and as a result, thicker catalyst layer was observed at the lumen rather than onto the conical-shaped microchannels. Therefore, the viscosity of catalyst solution and calcination process should be precisely controlled to ensure homogeneous catalyst layer deposition. Analysis of the elemental composition will be studied in the future using energy dispersive X-ray Spectroscopy (EDX) to determine the elements deposited onto the membranes. Once the elemental analysis is confirmed, oxygen permeation analysis will be carried out.

1 Introduction

Currently, industrial oxygen production relies on traditional technologies such as cryogenic distillation and pressure swing adsorption, which required a prohibitively large capital investment and high operating costs. Therefore, a potentially cheaper technology by using dense mixed ionic and electronic conducting (MIEC) ceramic membrane to separate oxygen from air is needed [1, 2]. Through oxygen enrichment of the combustion air with ceramic membranes, significant saving of energy can be expected due to enhanced combustion efficiency.

MIEC oxides are multifunctional materials that are widely used as catalysts [3], fuel cells electrodes [4], and oxygen permeation membranes [5]-[7]. In compared to the oxygen permeation over polymer-based membrane and industrial state-of-the-art method, the membranes developed using MIEC oxides have significant advantages such as simplified operation and high efficiency. Besides that, this MIEC dense membrane has 100% oxygen permeation selectivity at elevated temperatures. They allow only oxygen to diffuse through

vacancies in the crystal lattice, which is charge-compensated by intrinsic electronic conductivity. Thus, various applications behold such as for oxygen production and as well as many industrial processes that require constant supply of oxygen i.e, conversion of hydrocarbon (oxidative coupling methane [8], [9] and partial oxidation of methane to syngas [10]) and oxygen ion conductor fuel cell. Besides that, dense MIEC ceramic membranes exhibit both excellent thermal stability and high oxygen flux which is thus make them suitable in the field of energy production or in integrated coal gasification power station [11], [12].

The fundamental studies of these MIEC membranes started with the pioneering work from Teraoka and co-workers in 1980's [13]. Perovskite type membranes having MIEC have been considered as one of the attractive materials for the oxygen separation. They could produce pure oxygen without the need for electrodes and external electrical loadings. Among various types of perovskites, La$_{1-x}$Sr$_x$Co$_{1-y}$Fe$_y$O$_{3-\delta}$ (LSCF) has been considered as one of the promising materials due to its high oxygen permeation flux and stability. However,

improvement of oxygen permeation flux is still needed for future commercialization.

It is known that the overall oxygen transport through a dense MIEC membrane are controlled by two mechanisms; (1) surface exchange reactions at the membrane surfaces and (2) oxygen diffusion rate through the bulk membrane (Fig. 1). Thus, the oxygen diffusion rate across the membrane can be improved by using better MIEC materials and/or reducing the membrane thickness. Asymmetric membrane structures, where a thin layer of dense MIEC deposited onto porous substrates have been widely proposed in order to reduce the effect of bulk diffusion. However, as the membrane thickness decreases, the effects of surface exchange reaction become dominating. Several studies have investigated the effects of adding porous catalytic layers on either side or both sides of the membrane and most of them resulting higher oxygen flux. This is due to the modification of oxygen potential drops at gas-membrane interfaces and improvement of oxygen exchange rates by the catalytic layers [14]-[18].
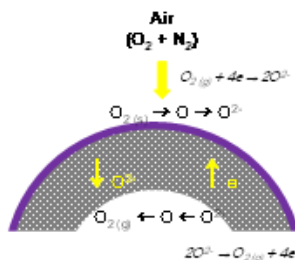

Figure 1. Mechanism of oxygen transport through dense MIEC

It has been realised that not all MIEC membranes are suitable to be fabricated into thin self-supported hollow fibre configuration due to mechanical strength and chemical stability. Among the perovskites materials under thoroughly studies are $La_{0.6}Sr_{0.4}Co_{0.2}Fe_{0.8}O_{3-\delta}$ (LSCF)[19, 20] and $Ba_{0.5}Sr_{0.6}Co_{0.2}Fe_{0.8}O_{3-\delta}$ (BSCF)[7, 21], which are very promising as oxygen separation membrane. In our previous works [9, 22], it was shown that a unique asymmetric structure of LSCF hollow fibre membrane, which consists of conical-shaped microchannels open at the inner surface and an outer dense oxygen separation can be prepared via a viscous fingering induced phase inversion. Not only this design has substantially reduced resistance across the membrane, but the open microchannels can act as a structured substrate where catalyst can be deposited/coated for enhancement of surface activity. As the surface area to volume ratio of this hollow fibre configuration is extremely high in compared to other configurations (disc & tubular), the performance of this membrane can greatly exceed that of other membrane systems. The thin hollow fibres also show a better mechanical stability in compared to disk-shaped membranes of the same wall thickness.

Fig. 2 shows a hollow fibre membrane with typical symmetric and asymmetric structures. The catalyst can be easily coated on the outer surface of the hollow membrane by using dip coating [23] or brushing

techniques[24]. However, for the micro-structured LSCF hollow fibre membrane with open microchannels, the techniques stated earlier were unlikely to provide uniform catalyst coating inside the lumen of the hollow fibre membrane. Therefore, a new vacuum-assisted technique for in-situ catalyst deposition has been proposed in the present work.
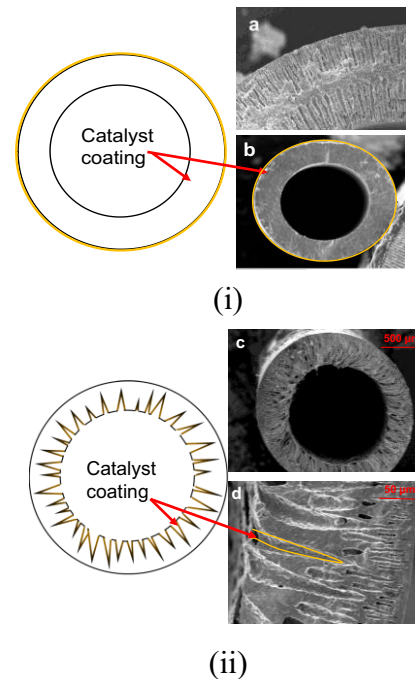

Figure 2. Surface modification of oxygen permeable membrane in (i) conventional a) asymmetric and b) symmetric structure and (ii) open microchannels structure (micro-structured).

2 Methodology

This work was divided into two main parts, which are preparation of the catalyst using sol-gel method and in-situ deposition of catalyst onto the micro-structured LSCF membrane microchannels using vacuum assisted techniques. The LSCF hollow fibre membrane used in this work was fabricated using a viscous fingering induced phase inversion process as described by Othman et al. Several characterization techniques such were then used to analyse the synthesized catalyst and surface-modified membrane.

2.1 Preparation of LSCF perovskites catalyst via sol-gel technique

The LSCF catalyst was prepared using the corresponding metal nitrates: $La(NO_3)_3.6H_2O$ (EMD Millipore) $Sr(NO_3)_{2v}$ (EMD Millipore,), $Co(NO_3)_2.6H_2O$ (Systerm ChemAR), and $Fe(NO_3)_3.9H2O$ (R&M Chemical). The starting solution was prepared by dissolving appropriate amounts of metal nitrate into distilled water by stirring at 80 °C. Citric acid and ethylene glycol were then added to the fully dissolved nitrate solution at the mole ratio of total metal ions: citric acid: ethylene glycol= 9: 3: 1. The

purpose of adding ethylene glycol is to inhibit cation segregation, resulting a homogeneous precursor solution. Then, the resultant solution was continuously stirred at 80 °C to accelerate polyesterification reaction of citric acid and ethylene glycol and continuous polymerization until a transparent brownish LSCF catalytic sol was formed. The LSCF catalytic sol was dried at 45 °C for 4 hours and 24 hours to investigate the effects of catalytic sol-viscosity. The LSCF sol was then calcinated at various calcination temperatures (600 – 900 °C) and heating rates (5.0 °C/min and 2.0 °C/min). Fig. 3 shows the scheme of LSCF preparation.
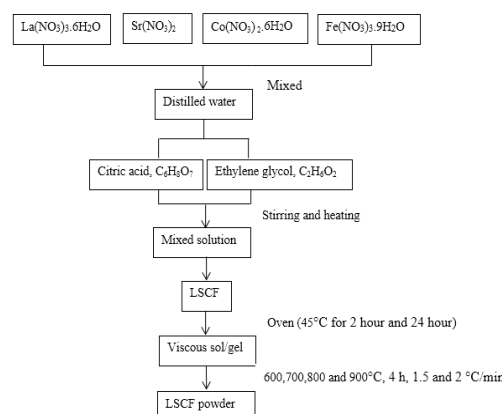

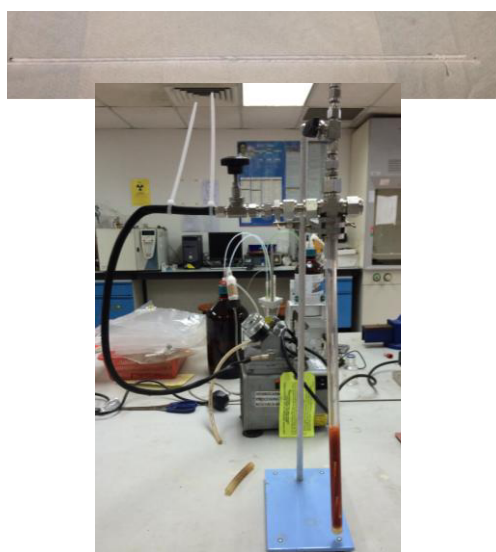**Figure 3.** Scheme of preparation of LSCF using sol-gel technique

Figure 4. Photograph on thee in-situ deposition of LSCF using vacuum-assisted technique

2.2 In-situ deposition of catalyst onto micro-structured LSCF oxygen permeable membrane

Prior to the deposition of catalysts, the micro-structured LSCF hollow fibre membranes thoroughly cleaned with water and acetone and dried in air. Then, the membranes were wrapped with PTFE tape to avoid any contamination on the outer surface of the hollow fibre during the coating. A vacuum assisted technique was used to improve the uniformity and controlled the

deposition of catalyst inside the lumen of LSCF hollow fibre membrane. The main function of the vacuum pump was to aid the removal of air inside the hollow fibre. Fig. 4 shows the in-house vacuum-depositor system used in this work. After the deposition, the fibres were dried at room temperature for 1 hour prior to calcination process.

2.3 Characterizations

The phase development of LSCF at different calcination temperatures and heating rates were analysed using X-ray diffractometer (XRD). The XRD patterns were obtained with an X'celerator detector (Rigaku) model using Cu-Kα as the radiation source. The XRD scans were carried out in 2θ which range from 10° to 80° using a step width of 0.05°. Thermogravimetric analysis of the synthesized catalysts was carried out by using a TG analyzer (Mettler Toledo) from room temperature to 1000 °C in air at a heating/cooling rate of 10 °C/min. The composition and purity of the synthesized. Both morphology and structure of the LSCF micro-structured hollow fibre membranes as well as the deposition of LSCF catalyst were observed by scanning electron microscopy (SEM) on HITACHI S-4800 (Japan).
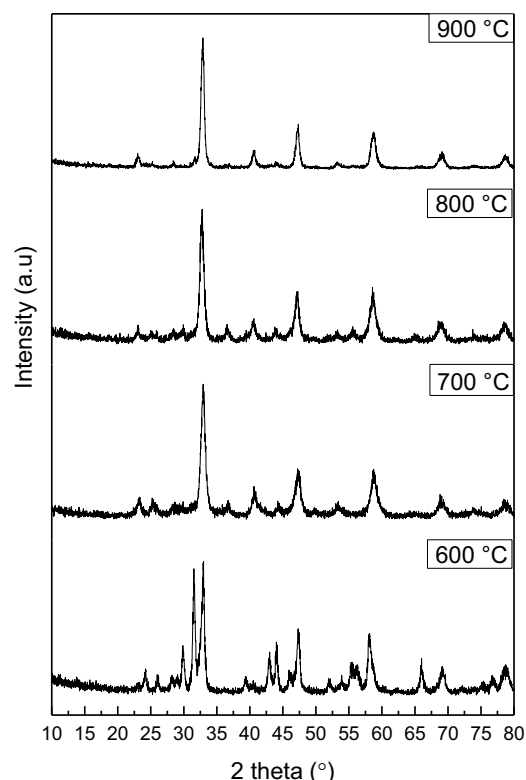

Figure 5. XRD powder patterns of LSCF powder calcined at 600-900°C

3 Results and discussions

3.1 Catalyst synthesis

3.1.1 LSCF

Calcination temperature could greatly affect the catalyst activity. A higher calcination temperature is usually required to obtain pure crystalline perovskite structure. However, with the increase of calcination temperatures the porosity and surface area of the perovskite catalyst could be reduced. Fig. 5 shows the effect of calcination temperatures on crystalline structure of LSCF at a heating rate of 5 º C/min. It can be seen that at higher temperature orthorhombic perovskite structure was obtained and at 900 °C, pure perovskite phase was developed by elimination of $SrCO_3$ [25]. In addition, the crystallinity of diffraction peaks was observed to increase with calcination temperatures. The higher intensity of the corresponding characteristic peaks of LSCF was due to the formation of larger crystalline particles after calcination process. The peaks of LSCF for were observed to shift slightly towards higher 2-theta values as the calcination temperatures increased. This indicates that the lattice diameter of LSCF decreases during the calcination process.

Thermal decomposition usually takes place in three stages. The first decomposition stage is at temperature around 100-250 ºC due to the loss of adsorbed water. At temperature between 300 to 750 ºC, second decomposition stages take place, which can be attributed to the burnout of organic components and third stages is the pyrolysis reaction may be due to complete dissociation of carbonates produced during combustion and initiation of the formation of LSCF phase. Fig. 6 shows the thermogravimetric analysis (TGA) curve of the calcined LSCF at various temperatures while Table 1 reports the mass loss values. The percentage of mass loss for the samples that were calcinated above 800 °C was found to be slightly lower (less than 4%) in compared to other samples because all the organics and impurities in the LSCF has been removed through calcination process. The small percentage of mass loss observed for temperature above 800 °C was believed as a result of $SrCO_3$ decomposition.

3.1.2 Effects of heating rate

In order to investigate the effect of heating rate, the LSCF sol were calcined at 800 °C using two different heating rates, which were 2 °C/min and 5 °C/min. Fig. 7 shows the XRD powder pattern of the calcinated LSCF powders. From the XRD pattern obtained, it is clearly shown that the formation of a single perovskite phase was affected by the heating rates used during the calcination process. At slower heating rate (2 °C/min), a clear crystalline perovskite structure can be formed at much lower temperature in compared to a faster heating rate (5 °C/min). This was because the sample has longer time to remove organic binder and impurities during heating up period [26]. Fig. 8 compares the amount of time required to complete the calcination process at 800 °C. The total calcination time when heating rate of 2 °C/min was used is 1010 minutes, while 548 minutes is required if a heating rate of 5 °C/min was used. This indicates that the shorter calcination time was not sufficient in removing the impurities, thus lead to an incomplete

perovskite structure. Therefore, by using slower heating rate, lower calcination temperature can be used.

Table 1 TGA weight loss percentage of LSCF

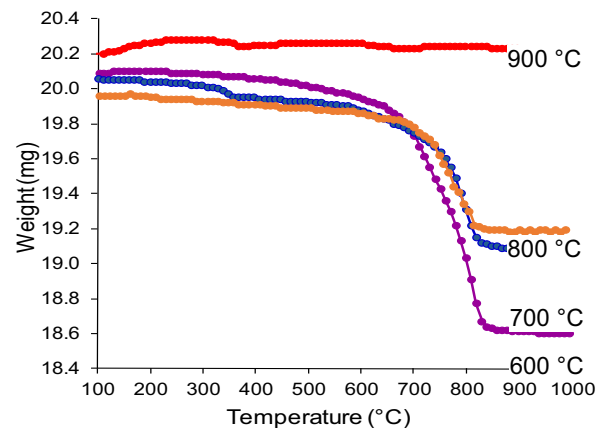| Calcination temperatures (°C)	Weight loss (%)
600	8.0
700	5.1
800	4.2
900	0.1

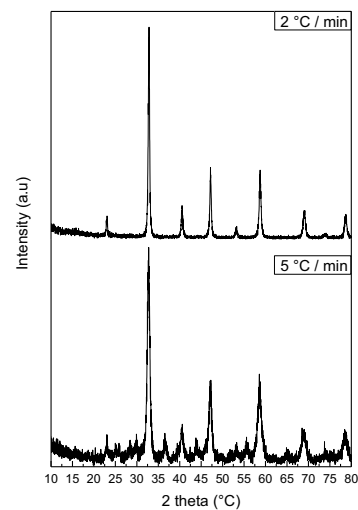**Figure 6.** TGA plot of LSCF calcined at 600-900 º C

Figure 7. XRD powder patterns of LSCF powder sintered at 800 ºC with 2 and 5 ºC/min heating rate.
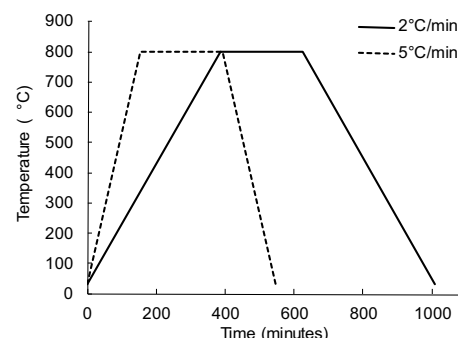

Figure 8. Total time required for the calcination process using heating rate of 2 °C/min and using 5 °C/min.

3.2 In-situ deposition of LSCF catalyst inside the micro-structured LSCF membrane

Viscosity of catalyst solutions plays a very role in order to obtain thin and homogeneous catalyst layer [27, 28]. If the catalyst sol is too low, the catalyst could not be deposited onto the membrane surface (dense membrane) or in a case of porous membrane, the catalyst sol will easily infiltrate into the membrane pores. Conversely, the use of highly viscous sol could lead to non-homogeneous deposition of catalyst that could lead to cracks of catalyst layer. The morphology and homogeneity of in-situ deposited LSCF catalyst was studied by SEM. Three different LSCF sol were used in this work. The viscosity of the sol was varied by increasing the evaporation time. The first sol (S1) used was without any evaporation, while the second sol (S2) and third sol (S3) was dried in an oven for 4 hours and 24 hours, respectively. After the deposition, LSCF membrane was calcined. Fig. 9 shows the SEM images of S1. A good coverage of catalyst onto the open conical-shaped microchannels was observed. However, if the depositing process is not properly controlled, there is a tendency of catalyst layer to crack and delaminated especially at the top of conical-shaped (Fig. 9a) and entrance (Fig. 9b) of microchannels.
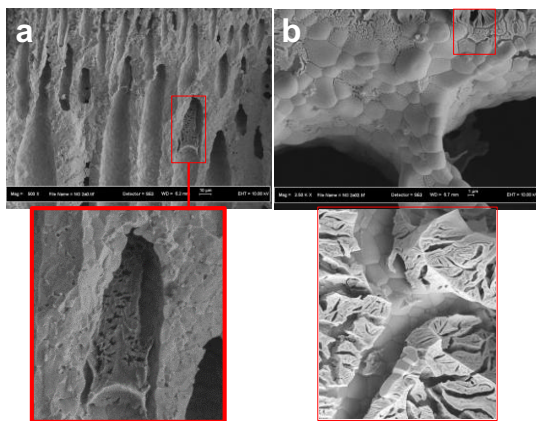

Figure 9. SEM photograph showing the surface morphology of S1 with a) top of conical-shaped microchannels and b) entrance of the microchannels.

Fig. 10 compares the SEM images of the in-situ deposited LSCF onto the micro-structured LSCF oxygen permeable membrane using the vacuum assisted technique. It can be seen clearly that the LSCF catalyst was successfully deposited without blocking the entrance to microchannels LSCF membrane. However, as the viscosity of the catalyst sol is higher (S3>S2>S1), uneven catalyst distribution across the membrane lumen can be seen. Interestingly, it was found that the amount of catalyst deposited using viscous solution was slightly higher than the less viscous sol. This might be due to the difficulty of catalyst sol to infiltrate the membrane and as a result, thicker catalyst layer was observed at the microchannels entrance rather than onto the conical-shaped microchannels (Fig. 10-S3). Therefore, the viscosity of catalyst solution and calcination process

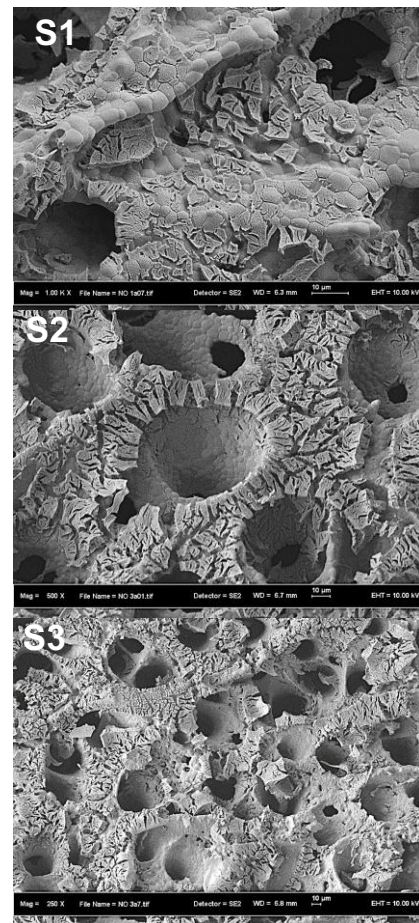should be precisely controlled in the future to ensure homogeneous catalyst layer deposition.

Figure 10. SEM photograph of in-situ deposited LSCF catalyst using three different catalytic sol evaporation time. S1) No evaporation, S2) 4 hours of evaporation and S3) 24 hours of evaporation

4 Conclusions

In this work, LSCF catalytic sol was first studied to investigate the effects of calcination temperature and heating rates towards the structure of LSCF. A pure perovskite structure is required to ensure high oxygen permeability. The LSCF sol was then deposited onto the unique asymmetric LSCF hollow fibre membrane, which consists of conical-shaped microchannels open at the inner surface and an outer dense oxygen separation. Due to the difficulty in obtaining thin and homogeneous catalyst layer by using conventional dip coating or brushing technique, a new vacuum-assisted technique for in-situ catalyst deposition was proposed. This preliminary study has confirmed the possibility of using the vacuum-assisted technique as one of the ways to deposited the catalyst. More details characterization such as analysis of elemental composition will be carried out in the future using energy dispersive X-ray Spectroscopy (EDX) to investigate the element deposited onto the membranes. Once the elemental analysis is confirmed, oxygen permeation analysis will be carried out.

Acknowledgement

References

1. J. Sunarso, et al., "Mixed ionic–electronic conducting (MIEC) ceramic-based membranes for oxygen separation," Journal of membrane science, vol. 320, pp. 13-41, 2008.
2. X. Tan, et al., "Mixed conducting ceramic hollow-fiber membranes for air separation," AIChE Journal, vol. 51, pp. 1991-2000, 2005.
3. Z. Q. Yu, et al., "Oxidative Coupling of Methane over Na2WO4/CeO2 and Related Catalysts," Journal of Catalysis, vol. 154, pp. 163-173, 1995.
4. T. Li, et al., "Single-step fabrication and characterisations of triple-layer ceramic hollow fibres for micro-tubular solid oxide fuel cells (SOFCs)," Journal of Membrane Science, vol. 449, pp. 1-8, 2014.
5. S. Engels, et al., "Oxygen permeation and stability investigations on MIEC membrane materials under operating conditions for power plant processes," Journal of membrane science, vol. 370, pp. 58-69, 2011.
6. G. Zhang, et al., "A novel Nb2O5-doped SrCo0.8Fe0.2O3−δ oxide with high permeability and stability for oxygen separation," Journal of membrane science, vol. 405–406, pp. 300-309, 2012.
7. Q. Jiang, et al., "Oxygen permeation study and improvement of Ba0.5Sr0.5Co0.8Fe0.2Ox perovskite ceramic membranes," Journal of membrane science, vol. 369, pp. 174-181, 2011.
8. O. Czuprat, et al., "Oxidative Coupling of Methane in a BCFZ Perovskite Hollow Fiber Membrane Reactor," Industrial & engineering chemistry research, vol. 49, pp. 10230-10236, Nov 3 2010.
9. N. H. Othman, et al., "A micro-structured La 0.6 Sr 0.4 Co 0.2 Fe 0.8 O 3− δ hollow fibre membrane reactor for oxidative coupling of methane," Journal of Membrane Science, vol. 468, pp. 31-41, 2014.
10. N. H. Othman, et al., "Bi1.5Y0.3Sm0.2O3-δ-based ceramic hollow fibre membranes for oxygenseparation and chemicalreactions," Journal of Membrane Science, vol. 432, pp. 58-65, 2013.
11. J. Tonziello and M. Vellini, "Oxygen production technologies for IGCC power plants with CO2 capture," Energy Procedia, vol. 4, pp. 637-644, 2011.
12. B. Jin, et al., "Plantwide control and operating strategy for air separation unit in oxy-combustion power plants," Energy Conversion and Management, vol. 106, pp. 782-792, 2015.
13. Y. Teraoka, "Mixed ionic-electronic conductivity of La1-xSrxCo1-yFeyO3-[delta] perovskite-type oxides," Materials research bulletin, vol. 23, p. 51, 1988.
14. Z. Wang, et al., "Improvement of the oxygen permeation through perovskite hollow fibre membranes by surface acid-modification," Journal of Membrane Science, vol. 345, pp. 65-73, 2009.
15. A. Leo, et al., "High performance perovskite hollow fibres for oxygen separation," Journal of membrane science, vol. 368, pp. 64-68, 2011.
16. V. V. Kharton, et al., "Surface modification of La0.3Sr0.7CoO3−δ ceramic membranes," Journal of Membrane Science, vol. 195, pp. 277-287, 2002.
17. A. Leo, et al., "Oxygen permeation through perovskite membranes and the improvement of oxygen flux by surface modification," Science and Technology of Advanced Materials, vol. 7, pp. 819-825, 2006.
18. L. Olivier, et al., "Oxidative coupling of methane using catalyst modified dense perovskite membrane reactors," Catalysis today, vol. 142, pp. 34-41, 2009.
19. X. Tan, et al., "Morphology control of the perovskite hollow fibre membranes for oxygen separation using different bore fluids," Journal of membrane science, vol. 378, pp. 308-318, 2011.
20. X. Tan, et al., "Oxygen production using La0.6Sr0.4Co0.2Fe0.8O3−α (LSCF) perovskite hollow fibre membrane modules," Journal of membrane science, vol. 310, pp. 550-556, 2008.
21. A. Leo, et al., "The enhancement of oxygen flux on Ba 0.5 Sr 0.5 Co 0.8 Fe 0.2 O 3− δ (BSCF) hollow fibers using silver surface modification," Journal of Membrane Science, vol. 340, pp. 148-153, 2009.
22. N. H. Othman, et al., "An oxygen permeable membrane microreactor with an in-situ deposited Bi 1.5 Y 0.3 Sm 0.2 O 3− δ catalyst for oxidative coupling of methane," Journal of Membrane Science, vol. 488, pp. 182-193, 2015.
23. H. Tikkanen, et al., "Examination of the co-sintering process of thin 8YSZ films obtained by dip-coating on in-house produced NiO-YSZ," Journal of the European Ceramic Society, vol. 31, pp. 1733-1739, Aug 2011.
24. V. Meille, "Review on methods to deposit catalysts on structured surfaces," Applied Catalysis A: General, vol. 315, pp. 1-17, 2006.
25. S. Liu, et al., "Synthesis and characterization of La0. 8Sr0. 2Co0. 5Fe0. 5O3±δ nanopowders by microwave assisted sol–gel route," Journal of Sol-Gel Science and Technology, vol. 44, pp. 187-193, 2007.
26. P. Bomlai, et al., "Effect of heating rate on the properties of Sb and Mn-doped barium strontium titanate PTCR ceramics," Materials Letters, vol. 59, pp. 118-122, 2005.
27. J. Bravo, et al., "Wall coating of a CuO/ZnO/Al 2 O 3 methanol steam reforming catalyst for micro-channel reformers," Chemical Engineering Journal, vol. 101, pp. 113-121, 2004.
28. R. Sonawane, et al., "Preparation and photo-catalytic activity of Fe TiO 2 thin films prepared by sol－gel dip coating," Materials Chemistry and Physics, vol. 85, pp. 52-57, 2004.